Biological Sciences: Biochemistry

Ferrous iron folds rRNA and mediates translation

Marcus S. Bray[a*], Tim K. Lenz[b*], Jessica C. Bowman[b], Anton S. Petrov[b], Amit R. Reddi[b], Nicholas V. Hud[b], Loren Dean Williams[b,1] and Jennifer B. Glass[c,1]

[a]School of Biological Sciences, Georgia Institute of Technology, 950 Atlantic Dr, Atlanta, GA, USA, 30332

[b]School of Chemistry and Biochemistry, Georgia Institute of Technology, 901 Atlantic Dr, Atlanta GA, USA, 30332

[c]School of Earth and Atmospheric Sciences, Georgia Institute of Technology, 311 Ferst Dr, Atlanta, GA, US, 30332

[*]These two people have contributed equally to this work.

[1]To whom correspondence should be addressed:
Jennifer B. Glass: School of Earth & Atmospheric Sciences, Georgia Institute of Technology, Atlanta, GA 30332; jennifer.glass@eas.gatech.edu; Tel. 404- 894-3942; Fax. 404-894-5638
Loren Dean Williams: School of Chemistry & Biochemistry, Georgia Institute of Technology, Atlanta, GA 30332; loren.williams@chemistry.gatech.edu; Tel. 404-385-6258; Fax. 404-894-2295

Keywords: Translation, SHAPE, iron, magnesium, ribosome, ribosome function, ribosome structure, protein synthesis

Running title: *Ferrous iron for rRNA folding and translation*

ABSTRACT

The ubiquity of Fe^{2+} in life, despite its insolubility in the presence of oxygen, appears to stem from conditions of the ancient Earth. Today, Mg^{2+} is an essential cofactor with diverse structural and functional roles in life's oldest macromolecular machine, the translation system. We tested whether anoxia and Fe^{2+} can revert the ribosome to a functional ancestral state. First, SHAPE (Selective 2'-Hydroxyl Acylation analyzed by Primer Extension) was used to compare the effect of Mg^{2+} vs. Fe^{2+} on the tertiary structure of rRNA. Then, we used *in vitro* translation reactions to test whether Fe^{2+} could mediate protein production, and quantified ribosomal iron content. We found that: (i) Fe^{2+} and Mg^{2+} had strikingly similar effects on rRNA folding; (ii) Fe^{2+} can replace Mg^{2+} as the dominant divalent cation during translation of mRNA to functional protein; (iii) Fe^{2+} associated extensively with the ribosome. Given that the translation system originated and matured when Fe^{2+} was abundant, these findings suggest that Fe^{2+} played a role in early ribosomal evolution.

SIGNIFICANCE

Ribosomes are found in every living organisms where they are responsible for the translation of messenger RNA into protein. The ribosome's centrality to cell function is underscored by its evolutionary conservation; the core structure has changed little since its inception ~4 billion years ago when ecosystems were anoxic and Fe^{2+}-rich. The ribosome is a model system for the study of bioinorganic chemistry, owing to the many highly coordinated divalent metal cations that are essential to its function. We studied the structure, function, and cation content of the ribosome under early Earth conditions, (high-Fe^{2+}, low-O_2). Our results expand the role of Fe^{2+} in ancient and extant biochemistry as a cofactor for ribosomal structure and function.

Life arose around 4 billion years ago on an anoxic Earth with abundant ferrous iron (1) [~1 mM Fe^{2+} in the ocean (2, 3)]. Biochemistry had access to this Fe^{2+} for over a billion years before molecular oxygen production by living organisms was sufficient to fully precipitate iron as rust. The pervasive use of Fe^{2+} in extant biochemistry, despite barriers to biological acquisition, likely stems from its importance in the evolution of the early biochemical systems.

The translation system, which synthesizes all coded protein (4), originated and matured during the Archean Eon (4-2.5 Ga; (5)) in high-Fe^{2+}, low-O_2 conditions. The common core of the ribosome, and many other aspects of the translation system, have remained essentially frozen since the last universal common ancestor (6, 7). In extant biochemistry, Mg^{2+} ions are essential for both structure and function of the ribosome (8, 9) and for functions of many enzymes involved in translation (10). In ribosomes, Mg^{2+} ions are observed in a variety of structural roles, including in rRNA-Mg^{2+} clamps (11) (**Fig. 1a**), in dinuclear Mg^{2+}-microclusters that frame the peptidyl transferase center (12) (**Fig. 1b**), and at the SSU-LSU interface (13) (**Fig. 1c**). Functional Mg^{2+} ions stabilize a critical bend in mRNA between the P-site and A-site codons (14) (**Fig. 1d**), and mediate rRNA-tRNA/mRNA interactions (15) (**Fig. 1e, f**). Accessory enzymes needed for translation – aminoacyl tRNA synthetases, methionyl-tRNA transformylase (MTF), creatine kinase, myokinase, and nucleoside-diphosphate kinase – also require Mg^{2+} ions as cofactors (**Table 1**).

Recent results support a model in which Fe^{2+}, instead of, or possibly along with Mg^{2+}, was a critical cofactor for ancient nucleic acid function. As predicted by this model, functional Mg^{2+}-to-Fe^{2+} substitutions under anoxic conditions were experimentally verified for RNA folding and ribozyme catalysis (16, 17), a DNA polymerase, a DNA ligase, and an RNA polymerase (18). Compared to Mg^{2+}, Fe^{2+} has been shown to more effectively 'activate' RNA. The phosphate affinity of Fe^{2+}, because of the lower energies of its d-orbitals, is slightly greater than that of Mg^{2+}. In first shell coordination complexes, the proximal phosphorus shows enhanced activation to nucleophilic attack. Therefore, for at least some nucleic acid processing enzymes, optimal activity is observed at lower concentrations of Fe^{2+} than Mg^{2+} (16, 18).

In this study, we relocated the translation system to the high-Fe^{2+}, low-O_2 environment of its ancient roots, and compared its structure, function, and cation content under modern vs. ancient conditions.

Results

Fe^{2+} folds LSU rRNA to a near-native state. To test whether Fe^{2+} can fold rRNA to a native-like state, we compared the folding of large subunit (LSU) rRNA in the presence of Fe^{2+} or Mg^{2+} by SHAPE (Selective 2'-Hydroxyl Acylation analyzed by Primer Extension). SHAPE provides quantitative, nucleotide resolution information about flexibility, base pairing and 3D structure, and has previously been used to monitor the influence of cations, small molecules, or proteins on RNA structure (20-24). We previously used SHAPE to show that the LSU rRNA adopts a near-native state in the presence of Mg^{2+}, with the core inter-domain architecture of the assembled ribosome and residues positioned for interactions with rProteins (19). In this study, SHAPE experiments were performed in an anoxic chamber to maintain the oxidation state and solubility of Fe^{2+}. The minimum concentration required to fold rRNA, 2.5 mM Fe^{2+} or 10 mM Mg^{2+}, was used for all SHAPE experiments (**Table S1**).

Addition of Fe^{2+} or Mg^{2+} induced widespread structural changes in the LSU rRNA, reflected in SHAPE reactivity as ΔFe^{2+} or ΔMg^{2+} (see **Materials and Methods**) and displayed as 'heat maps' on the LSU rRNA secondary structure (**Fig. 2**). The ΔFe^{2+} and ΔMg^{2+} heat maps were broadly similar at the nucleotide and regional scale (**Fig. 2d**, **e**). Helical regions tended to be invariant, whereas addition of Fe^{2+} or Mg^{2+} induced numerous changes to unpaired nucleotides, including rRNA loops and bulges. Of the sites that exhibited a significant response (>0.3 SHAPE units) to Mg^{2+}, 86% of nucleotides (43/50) exhibited a similar trend with Fe^{2+}. The greatest discrepancy between Fe^{2+} and Mg^{2+} is observed in the L11 binding domain.

83 ***Fe^{2+} and Mn^{2+} mediate translation.*** Translation reactions were performed in the anoxic chamber in the
84 presence of different divalent cations and cation concentrations (**Fig. S1**). Production of dihydrofolate
85 reductase (DHFR) from its cognate mRNA was used to monitor translational activity. Protein synthesis was
86 assayed by measuring the rate of NADPH oxidation by DHFR. All reactions were conducted in a small
87 background of 2.5 mM Mg^{2+}. This background is below the requirement to support translation, consistent
88 with previous findings that a minimum of ~5 mM Mg^{2+} is needed for assembly of mRNA onto the SSU
89 (25-27). As a control, we recapitulated the previously established Mg^{2+} dependence of the translation
90 system, and then repeated the assay with Fe^{2+}.
91
92 The activity profile of the translation system with varied Fe^{2+} closely tracked the profile with varied Mg^{2+}
93 (**Fig. 3**). Below 7.5 mM total divalent cations, minimal translation occurred with either Fe^{2+} or Mg^{2+}, as
94 observed elsewhere (28). Activity peaked at 9.5 mM for both cations and decreased modestly beyond the
95 optimum. At a given divalent cation concentration, Fe^{2+} supported around 50-80% of activity with Mg^{2+}.
96 This result was observed with translation reactions run for 15, 30, 45, 60, 90 and 120 min with optimal
97 divalent cation concentrations (**Fig. 4**). Along with Mg^{2+} and Fe^{2+}, we investigated the abilities of other
98 divalent cations to support translation, including Mn^{2+}, Co^{2+}, Cu^{2+}, and Zn^{2+}. We found that Mn^{2+} supported
99 translation at levels similar to Fe^{2+}, whereas no activity was detected with Co^{2+}, Cu^{2+}, or Zn^{2+} (**Fig. 5**).
100
101 ***Fe^{2+} associates extensively with the ribosome.*** To experimentally confirm that Fe^{2+} associates with the
102 assembled ribosome, we analyzed the Fe^{2+} content of ribosomes after incubation in anoxic reaction buffer
103 containing 7 mM Fe^{2+}. We observed that under the conditions of our translation reactions, 584 ± 9 Fe^{2+} ions
104 associate with each ribosome.
105
106 **Discussion**

107 In this study, we successfully replaced ribosomal Mg^{2+} with Fe^{2+} under conditions mimicking the anoxic
108 Archean Earth. Previously, the only cation known to mediate folding and function of the translation system
109 was Mg^{2+}. We found that rRNA folds to the same extent, and to essentially the same global state (39, 40),
110 with Fe^{2+} or Mg^{2+} under anoxia. The minimum concentration of Fe^{2+} required to fold the rRNA is 4-fold
111 less than the requisite Mg^{2+} concentration. We also showed that Fe^{2+} or Mn^{2+} can mediate translation as the
112 dominant divalent cation in place of Mg^{2+} at >6 mM. These findings suggest that functional Mg^{2+}-Mn^{2+}-
113 Fe^{2+} substitutions occur in ribozymes, similar to previous reports for protein enzymes (29, 30). The
114 effectiveness of these ion substitutions in the translation system is astounding considering the enormous
115 number of divalent cations, and the diversity of their structural and functional roles (8-10) (**Table 1, Fig.**
116 **1**).

117 The observation of >500 Fe^{2+} ions associated with each ribosome verifies that Fe^{2+} can interact extensively
118 with the ribosome. This result is consistent with the extent of Mg^{2+} association observed by x-ray diffraction
119 (100-1000 Mg^{2+} per ribosome (31, 32)), and supports a model in which Fe^{2+} has replaced Mg^{2+} as the
120 dominant divalent cation in our experiments. The high capacity of ribosomes for Fe^{2+} reflects all ribosome-
121 associated ions, in condensed, glassy and chelated states (33).

122 For *E. coli* and other microbes, intracellular Mg^{2+} closely reflects extracellular Mg^{2+} concentrations (8), and
123 intracellular Fe^{2+} is limiting in oxic conditions (34). Infectious microbes confront high iron environments
124 in the context of iron-overload disorders (35). In certain hypoxic environments, intracellular Fe^{2+} may
125 effectively compete with Mg^{2+} as the dominant intracellular divalent cation. It is possible that the absence
126 of Fe^{2+} in experimentally determined ribosomal structures is reflective of culturing and purification
127 conditions (high Mg^{2+}, high O_2, and low Fe^{2+}) rather than a physiological requirement.

128 The complexity of the ribosome, and the translation system in general, suggest that differences in activity
129 with Fe^{2+} vs. Mg^{2+} arise from a variety of evolutionary, biochemical, and physiological factors. It is possible
130 that one or more of the accessory enzymes in **Table 1** have lower activity in the presence of Fe^{2+} than Mg^{2+},
131 and/or that the oxic, low-Fe^{2+} conditions under which the commercial ribosomes were grown and/or purified

132 primed them for higher activity with Mg^{2+} vs. Fe^{2+}. It is also possible that Fe^{2+}-containing ribosomes are
133 less active due to Fe^{2+}-mediated damage to RNA, as shown for Fe^{2+}-containing ribosomes from Alzheimer
134 hippocampus (36). Further work is required to investigate efficiencies of ribosomes and other translation
135 components prepared under anoxic, Fe^{2+}-rich conditions.

136 When combined with previous results that DNA replication and transcription can be facilitated by Fe^{2+} (18),
137 our finding that Fe^{2+} can mediate rRNA folding and translation of mRNA to protein has revealed that Fe^{2+}
138 can facilitate the entire central dogma of molecular biology (DNA→RNA→protein). This finding raises
139 important questions about evolutionary and physiological roles for Fe^{2+} in ancient and extant biological
140 systems. Were Mg^{2+} and Fe^{2+} collaborators as cofactors on the ancient Earth, when both ions were present
141 in the low-mM range (2, 3)? What was the role of Fe^{2+} in the origin and early evolution of the translational
142 system? Finally, what are the implications for ribosome-bound Fe^{2+} in oxidative damage and disease?

143 **Materials and Methods**
144
145 **rRNA folding via SHAPE.** SHAPE methods were adapted from previously published protocols (19) using
146 the intact ~2900 nt *T. thermophilus* 23 rRNA (LSU) in the presence of 250 mM Na^+, which favors formation
147 of secondary structure, and in 250 mM Na^+ plus a divalent cation (10 mM Mg^{2+} or 2.5 mM Fe^{2+}, both as
148 chloride salts) to favor formation of tertiary interactions. Adaptations were made to facilitate folding and
149 N-methylisatoic anhydride modification of RNA in an anoxic chamber under a 98% Ar and 2% H_2
150 atmosphere. To keep rRNA samples oxygen-free, rRNA samples in 200 mM NaOAc, 50 mM NaHEPES
151 (pH 8) were lyophilized, transferred into the anoxic chamber, and rehydrated with nuclease-free, degassed
152 water. After rRNA modification as described in ref. (19), divalent cations were extracted from the rRNA
153 by chelating beads. Samples were then removed from the anoxic chamber for analysis by capillary
154 electrophoresis (19). Nucleotides were classified as exhibiting a significant change in SHAPE reactivity if
155 either the original reactivity (in Na^+) or final reactivity (in Na^+/Mg^{2+} or Na^+/Fe^{2+}) was >0.3 SHAPE units.
156 To compare the Fe^{2+}- and Mg^{2+}-responsiveness of specific nucleotides, we binned nucleotides into three
157 categories (increased, decreased, or little/no change) based on their general SHAPE reactivity response to
158 each divalent cation (SHAPE data are found in **Table S1**). This method allowed us to interrogate structural
159 changes induced by Mg^{2+} or Fe^{2+}.

160 ***In vitro* translation.** Each 30 μL reaction contained 2 μM (4.5 μL of 13.3 μM stock) *E. coli* ribosomes in
161 10 mM Mg^{2+} (New England Biolabs, Ipswich MA, USA; catalog # P0763S), 3 μL factor mix (with RNA
162 polymerase, and transcription/translation factors in 10 mM Mg^{2+}) from the PURExpress® Δ Ribosome Kit
163 (New England Biolabs E3313S), 0.1 mM amino acid mix (Promega, Madison WI, USA; catalog # L4461),
164 and 0.2 mM tRNAs from *E. coli* MRE 600 (Sigma-Aldrich, St. Louis MO, USA; product # TRNAMRE-
165 RO). Thus, a total of 2.5 mM "background" Mg^{2+} was present in each reaction (**Fig. S1**). The background
166 is unavoidable because ribosomes and accessory enzymes are produced *in vivo* in the presence of Mg^{2+}, and
167 removal of all Mg^{2+} by long dialysis under anoxic conditions is technically infeasible.
168
169 **Translation reaction buffer.** The reaction buffer was based on Shimizu et al. (37), with HEPES-OH
170 instead of phosphate buffer to avoid precipitation of metal phosphates. Tris-HCl was also tested as a buffer,
171 but rates of translation were consistently lower with Tris-HCl than HEPES-OH, and therefore HEPES-OH
172 was used as the buffer for all experiments. Buffer consisted of 20 mM HEPES-OH (pH 7.3), 95 mM
173 potassium glutamate, 5 mM ammonium chloride, 0.5 mM calcium chloride, 1 mM spermidine, 8 mM
174 putrescine, 1 mM dithiothreitol (DTT), 2 mM adenosine triphosphate (ATP), 2 mM guanosine triphosphate
175 (GTP), 1 mM uridine triphosphate (UTP), 1 mM cytidine triphosphate (CTP), 10 mM creatine phosphate
176 (CP), and 53 μM 10-formyltetrahydrofolate. The reaction buffer was lyophilized and stored at -80°C until
177 resuspension in anoxic nuclease-free water immediately before experiments in the anoxic chamber.
178
179 **DNA and mRNA templates**. A plasmid containing the gene encoding dihydrofolate reductase (DHFR)
180 from *E. coli* was provided as a gift from New England Biolabs. DHFR control plasmid was linearized using

HindIII restriction enzyme, purified by phenol/chloroform extraction, precipitated in ethanol, and resuspended in nuclease-free water. Messenger RNA was generated using the HiScribe™ T7 High Yield RNA Synthesis Kit (New England Biolabs catalog # E2040S) and purified using the MEGAclear™ Transcription Clean-Up Kit (Thermo Fisher, Waltham MA, USA; catalog # AM1908).

Translation experimental conditions. All reactions (30 µL total volume) were assembled and incubated in the anoxic chamber. All divalent cation salts used in experiments ($MgCl_2$, $FeCl_2$, $MnCl_2$, $Zn(OAc)_2$, $CoCl_2$, $CuSO_4$) were added to 7 mM final concentration, with the exception of $MgCl_2$ and $FeCl_2$, which were tested over a range of final concentrations (1, 3, 4, 5, 6, 7, 8, 9, and 11 mM; **Fig. S1**). All experiments were assembled in the following order: mRNA (~5 µg per 30 µL reaction), factor mix, ribosomes, amino acids, tRNA, nuclease-free H_2O, reaction buffer. Changing the order of reactant addition did not affect translational activity. Reactions were run in triplicate on a 37°C heat block for up to 120 minutes. Reactions were quenched on ice and stored at 4°C on ice until assay for protein synthesis.

Protein activity assay. Protein synthesis was measured using a dihydrofolate reductase (DHFR) assay kit (Sigma-Aldrich product # CS0340), which measures the oxidation of NADPH (60 mM) to $NADP^+$ by dihydrofolic acid (DHFA; 51.25 µM). Assays were performed by adding 5 µL of protein synthesis reaction to 995 µL of 1x assay buffer. The NADPH absorbance peak at 340 nm (Abs_{340}) was measured in 15 s intervals over 2.5 min. The slope of the linear regression of Abs_{340} vs. time was used to determine protein activity (Abs_{340} min^{-1}). Different counter ions (Cl^-, CH_3COO^-, SO_4^{2-}) had no effect on protein synthesis from mRNA. To our knowledge, no dependence on, nor inhibitory effect of, Mg^{2+} or Fe^{2+} exists for DHFR. We confirmed this by varying the amounts of metals in our assay reaction, which had no effect on DHFR activity (data not shown).

Ribosome iron content. In order to measure the iron content of ribosomes, a 300 µL reaction was prepared containing 45 µL of a 13.3 µM stock of *E. coli* ribosomes (New England Biolabs catalog # P0763S), 7 mM $FeCl_2$, and reaction buffer. These reactions were scaled up to 10x volume, which was necessary due to technical constraints on spin columns. Blank samples with 7 mM $FeCl_2$ and reaction buffer, but without ribosomes, were also prepared. All mixtures were incubated at 37°C for 2 hours. After incubation, samples were transferred to Vivaspin 500 centrifugal concentrators (Vivaproducts, Littleton, MA; catalog # VS0141) and spun at 15,000 x g until minimum retentate volume (~5 µL) was achieved. Retentate was transferred to a 1.5 mL microcentrifuge tube and suspended in 200 µL of 10 mM HEPES-OH (pH 7.3, 50 mM NaCl). Samples were spiked with 1 ppm Ga concentration standard, and 2 µL were dried on siliconized quartz discs. Metal analysis was performed by total reflection x-ray fluorescence (TRXF) spectroscopy (S2 Picofox TRXF spectrometer; Bruker, Billerica, MA). Samples were run at 50 kV for 2000 s each. TRXF spectra were used to calculate the concentration of Fe in mg L^{-1}. Blank values were subtracted from ribosome samples and these corrected concentrations were converted to mM. The final ribosomal concentration (3 µM) was based on our dilution of NEB ribosomes supplied at 13.3 µM using RNA absorbance at 260 nm ($1A_{260}$ = 60 µg mL^{-1}). Values were reported as moles of Fe^{2+} per mole ribosome ± standard error of the mean of triplicate experiments.

ACKNOWLEDGMENTS. This research was supported by the National Aeronautics and Space Administration grants NNX14AJ87G, NNX16AJ28G, and NNX16AJ29G. We acknowledge helpful discussions with Corinna Tuckey of New England Biolabs, and with Eric B. O'Neill and Claudia Montllor Albalate of Georgia Institute of Technology. We thank Michael Goodisman for access to a capillary electrophoresis instrument.

Competing interests. The authors declare that they have no competing interests with the contents of this article.

Author contributions: MSB, TKL, JCB, ARR, NVH, LDW, and JBG conceived and designed the experiments. MSB and TKL collected data and performed analysis. ASP contributed analysis. MSB, TKL, LDW, and JBG wrote the paper with editorial input from all authors.

References

1. Poulton SW & Canfield DE (2011) Ferruginous conditions: A dominant feature of the ocean through earth's history. *Elements* 7(2):107-112.
2. Derry LA (2015) Causes and consequences of mid-Proterozoic anoxia. *Geophys Res Lett* 42(20):8538-8546.
3. Jones C, Nomosatryo S, Crowe SA, Bjerrum CJ, & Canfield DE (2015) Iron oxides, divalent cations, silica, and the early earth phosphorus crisis. *Geology* 43(2):135-138.
4. Ramakrishnan V (2002) Ribosome structure and the mechanism of translation. *Cell* 108(4):557-572.
5. Fox GE (2010) Origin and evolution of the ribosome. *Cold Spring Harb Perspect* 2(9):a003483.
6. Koonin EV (2003) Comparative genomics, minimal gene-sets and the last universal common ancestor. *Nature Rev Microbiol* 1(2):127.
7. Charlebois RL & Doolittle WF (2004) Computing prokaryotic gene ubiquity: Rescuing the core from extinction. *Genome Res* 14(12):2469-2477.
8. Hurwitz C & Rosano CL (1967) The intracellular concentration of bound and unbound magnesium ions in *Escherichia coli*. *J Biol Chem* 242(16):3719-3722.
9. Klein DJ, Moore PB, & Steitz TA (2004) The contribution of metal ions to the structural stability of the large ribosomal subunit. *RNA* 10(9):1366-1379.
10. Cusack S (1997) Aminoacyl-tRNA synthetases. *Curr Opin Struct Biol* 7(6):881-889.
11. Petrov AS, Bowman JC, Harvey SC, & Williams LD (2011) Bidentate RNA–magnesium clamps: On the origin of the special role of magnesium in RNA folding. *RNA* 17(2):291-297.
12. Hsiao C & Williams LD (2009) A recurrent magnesium-binding motif provides a framework for the ribosomal peptidyl transferase center. *Nucleic Acid Res* 37(10):3134-3142.
13. Schuwirth BS*, et al.* (2005) Structures of the bacterial ribosome at 3.5 Å resolution. *Science* 310(5749):827-834.
14. Demeshkina N, Jenner L, Westhof E, Yusupov M, & Yusupova G (2012) A new understanding of the decoding principle on the ribosome. *Nature* 484(7393):256.
15. Selmer M*, et al.* (2006) Structure of the 70S ribosome complexed with mRNA and tRNA. *Science* 313(5795):1935-1942.
16. Athavale SS*, et al.* (2012) RNA folding and catalysis mediated by iron (II). *PLoS One* 7(5):e38024.
17. Popović M, Fliss PS, & Ditzler MA (2015) *In vitro* evolution of distinct self-cleaving ribozymes in diverse environments. *Nucleic Acids Res* 43(14):7070-7082.
18. Okafor CD*, et al.* (2017) Iron mediates catalysis of nucleic acid processing enzymes: Support for Fe (II) as a cofactor before the great oxidation event. *Nucleic Acids Res* 45(7):3634-3642.
19. Lenz TK, Norris AM, Hud NV, & Williams LD (2017) Protein-free ribosomal RNA folds to a near-native state in the presence of Mg^{2+}. *RSC Adv*:DOI 10.1039/c1037ra08696b.
20. Dann III CE*, et al.* (2007) Structure and mechanism of a metal-sensing regulatory RNA. *Cell* 130(5):878-892.
21. Mortimer SA & Weeks KM (2007) A fast-acting reagent for accurate analysis of RNA secondary and tertiary structure by SHAPE chemistry. *J Am Chem Soc* 129(14):4144-4145.
22. Athavale SS*, et al.* (2012) Domain III of the *T. thermophilus* 23S rRNA folds independently to a near-native state. *RNA* 18(4):752-758.
23. Hsiao C*, et al.* (2013) Molecular paleontology: A biochemical model of the ancestral ribosome. *Nucleic Acids Res* 41(5):3373-3385.
24. Lanier KA, Athavale SS, Petrov AS, Wartell RM, & Williams LD (2016) Imprint of ancient evolution on rRNA folding. *Biochemistry* 55(33):4603-4613.

25. Takanami M & Okamoto T (1963) Interaction of ribosomes and synthetic polyribonucleotides. *J Mol Biol* 7(4):323-333.
26. Kigawa T*, et al.* (1999) Cell-free production and stable-isotope labeling of milligram quantities of proteins. *FEBS Lett* 442(1):15-19.
27. Goldberg A (1966) Magnesium binding by *Escherichia coli* ribosomes. *J Mol Biol* 15(2):663-673.
28. Pronczuk A, Baliga B, & Munro H (1968) Effect of nucleoside triphosphate and magnesium ion concentration on the stability and function of rat liver polysomes *in vitro*. *Biochem J* 110(4):783-788.
29. Bock CW, Katz AK, Markham GD, & Glusker JP (1999) Manganese as a replacement for magnesium and zinc: Functional comparison of the divalent ions. *J Amer Chem Soc* 121(32):7360-7372.
30. Imlay JA (2014) The mismetallation of enzymes during oxidative stress. *J Biol Chem* 289(41):28121-28128.
31. Zheng H, Shabalin IG, Handing KB, Bujnicki JM, & Minor W (2015) Magnesium-binding architectures in RNA crystal structures: Validation, binding preferences, classification and motif detection. *Nucleic Acids Res* 43(7):3789-3801.
32. Rodgers A (1964) The exchange properties of magnesium in *Escherichia coli* ribosomes. *Biochem J* 90(3):548-555.
33. Bowman JC, Lenz TK, Hud NV, & Williams LD (2012) Cations in charge: Magnesium ions in RNA folding and catalysis. *Curr Opin Struct Biol* 22(3):262-272.
34. Beauchene NA*, et al.* (2017) O_2 availability impacts iron homeostasis in *Escherichia coli*. *Proc Natl Acad Sci* 14 (46):12261-12266.
35. Cassat JE & Skaar EP (2013) Iron in infection and immunity. *Cell Host Microbe* 13(5):509-519.
36. Honda K*, et al.* (2005) Ribosomal RNA in Alzheimer disease is oxidized by bound redox-active iron. *J Biol Chem* 280(22):20978-20986.
37. Shimizu Y*, et al.* (2001) Cell-free translation reconstituted with purified components. *Nature Biotechnol* 19(8):751.
38. Bernier CR*, et al.* (2014) RiboVision suite for visualization and analysis of ribosomes. *Faraday Disc* 169:195-207.
39. Brion P & Westhof E (1997) Hierarchy and dynamics of RNA folding. *Annu Rev Biophys Biomol Struct* 26:113-137.
40. Tinoco I, Jr. & Bustamante C (1999) How RNA folds. *J Mol Biol* 293(2):271-281.

Table 1. Structural and functional roles for select divalent cations in the translation system. All biomolecules in the table have been shown to require Mg^{2+}, and may also be active with Fe^{2+}. "n.a." indicates that data are not available.

Translation system component(s)	Location of divalent ion	Role of divalent cation	Optimal [Mg^{2+}] (mM)
Ribosome			
LSU/SSU	rRNA-Mg^{2+} clamps (11)	Mediates and maintains folding/structure of rRNAs	~10 (20)
LSU	Mg^{2+} microclusters (12)	Frames peptidyl transferase center	~10 (20)
LSU/SSU	SSU-LSU interface (32)	Mediates docking of mRNA to SSU and association of SSU with LSU	~10 (20)
SSU/mRNA	Critical bend in mRNA between the P-site and A-site codons (15)	Maintains correct reading frame mRNA	~10 (20)
LSU/tRNA	rRNA-tRNA interactions (32)	Stabilize rRNA-tRNA in the PTC	~10 (20)
A-site tRNA/ P-site tRNA	tRNA-tRNA interactions (32)	Stabilize tRNAs in the PTC	~10 (20)
Auxiliary			
EF-Tu	GTP binding site (33)	Stabilizes the transition state	n.a.
EF-G	GTP binding site (34)	Stabilizes the transition state	n.a.
Aminoacyl-tRNA synthetases	ATP binding site (35)	Stabilizes the transition state	>1 (36)
Methionyl-tRNA transformylase	ATP binding site (37)	Stabilizes the transition state	7 (37)
Creatine kinase	NTP binding site (38)	Stabilizes the transition state	~5 (38)
Myokinase	Acceptor NDP binding site (39)	Stabilizes the transition state	n.a.
Nucleoside-diphosphate kinase	NTP binding site (40)	Stabilizes the transition state	>1
Pyrophosphatase	Active site (41)	Stabilizes the transition state	>7 (42)

314

315 **Figure Captions**
316
317 **Figure 1.** Divalent cations serve many structural and functional roles in the ribosome. Mg^{2+} ions: **a)** form
318 bidentate clamps with adjacent phosphate groups of rRNA (beige carbon atoms), **b)** form dinuclear
319 microclusters that frame the rRNA of the peptidyl transferase center, **c)** stabilize the LSU-SSU interface,
320 **d)** stabilize a functional kink in mRNA (green), **e)** stabilize association of tRNA (teal) with 23S rRNA, and
321 **f)** stabilize association of mRNA with 16S rRNA. Thick dashed lines are first shell RNA interactions of
322 Mg^{2+}. Dotted lines indicate second shell interactions. Images are of the *Thermus thermophilus* ribosome
323 (PDB ID: 1VY4) because the structural information available for *T. thermophilus* ribosomes is more
324 accurate than for *E. coli*. This figure was generated with the program RiboVision (38).

325 **Figure 2.** SHAPE reactivities mapped onto the LSU rRNA secondary structure in **a)** Na^+, **b)** Na^+/Fe^{2+}, or
326 **c)** Na^+/Mg^{2+}. The scale shown for panel a applies to panels b and c. **d)** Fe^{2+}-induced changes (ΔFe^{2+}) in
327 SHAPE reactivity calculated by subtracting Na^+ data from Na^+/Fe^{2+} data for each nucleotide, and **e)** Mg^{2+}-
328 induced changes (ΔMg^{2+}) in SHAPE reactivity calculated by subtracting Na^+ data from Na^+/Mg^{2+} data for
329 each nucleotide. The scale shown for panel d also applies to panel e. Positive values indicate increased
330 SHAPE reactivity in presence of the divalent cation, while negative values denote decreased reactivity.
331 Regions where data are not available (5' and 3' ends) are grey. These figures were generated with the
332 program RiboVision (38). *Thermus thermophilus* rRNA was used as the analytical model for SHAPE
333 experiments because the structural information is more accurate than for *E. coli*.

334 **Figure 3**. Mg^{2+} and Fe^{2+} stimulate translational activity over a range of concentrations. The activity of the
335 translation product (dihydrofolate reductase, which catalyzes the oxidation of NADPH, with a maximum
336 absorbance at 340 nm) was used as a proxy for protein production. Translation reactions were run for 120
337 minutes. All translation reactions contained 2.5 mM background Mg^{2+}, to which varying amounts of
338 additional Mg^{2+} or Fe^{2+} were added. The error bars for triplicate experiments (N=3) are plotted as the
339 standard error of the mean.

340 **Figure 4.** Fe^{2+} consistently supports 50-80% of the translational activity as Mg^{2+} when the translation
341 experiments are run for 15-120 minutes. The activity of the translation product (dihydrofolate reductase,
342 which catalyzes the oxidation of NADPH, with a maximum absorbance at 340 nm) was used as a proxy for
343 protein production. All translation reactions contained 2.5 mM background Mg^{2+}, to which 7 mM additional
344 Mg^{2+} or Fe^{2+} were added, totaling to 9.5 mM divalent cation. The error bars for triplicate experiments (N=3)
345 are plotted as the standard error of the mean.

346 **Figure 5.** *In vitro* translation of active protein in the presence of different divalent cations (M^{2+}). The
347 activity of the translation product (dihydrofolate reductase, which catalyzes the oxidation of NADPH, with
348 a maximum absorbance at 340 nm) was used as a proxy for protein production. Treatments received 7 mM
349 M^{2+}, in addition to 2.5 mM background Mg^{2+}, summing to 9.5 mM total divalent cations. Translation
350 reactions were run for 120 minutes. The error bars for triplicate experiments (N=3) are plotted as the
351 standard error of the mean.

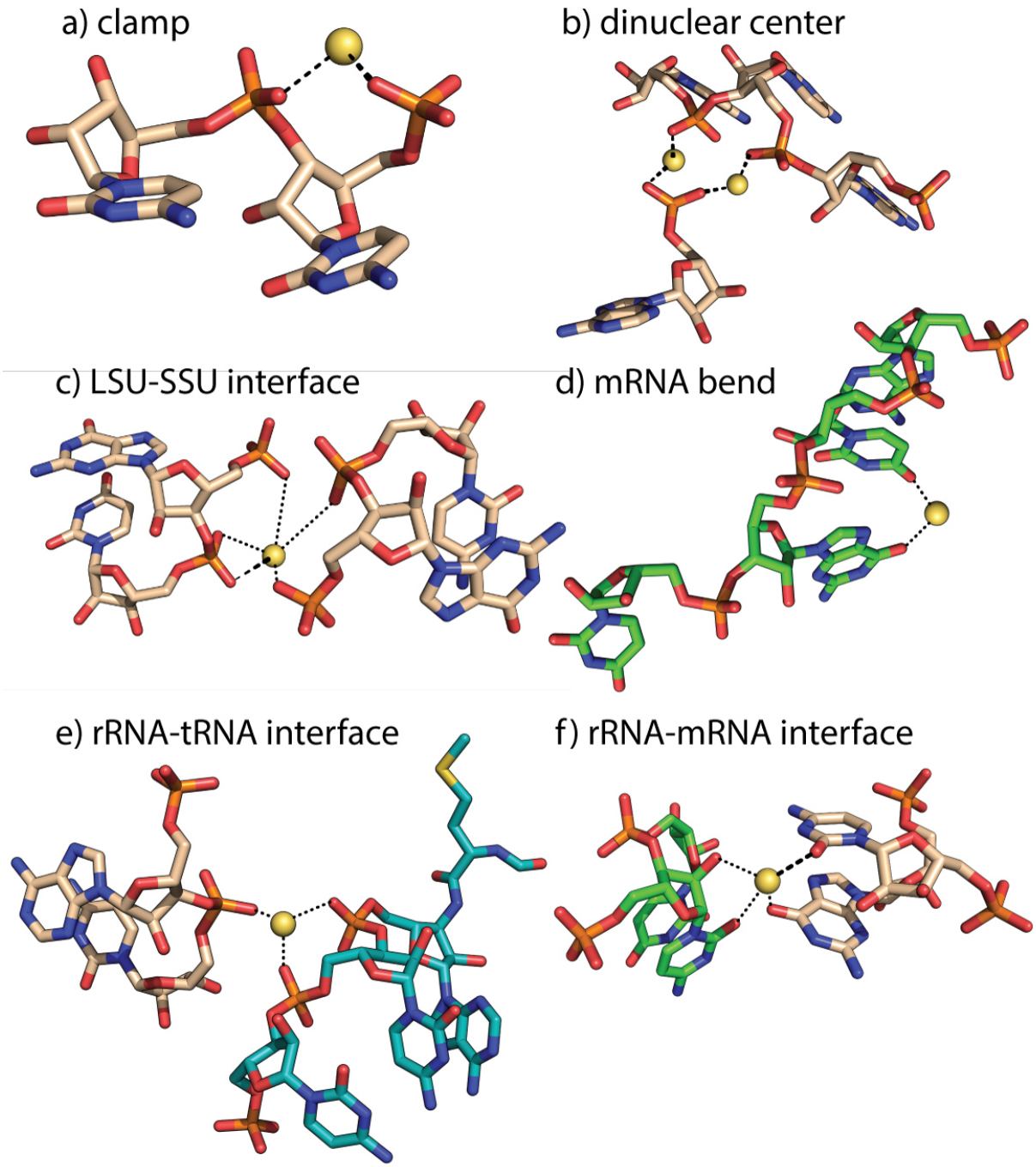
a) clamp
b) dinuclear center
c) LSU-SSU interface
d) mRNA bend
e) rRNA-tRNA interface
f) rRNA-mRNA interface

Figure 1

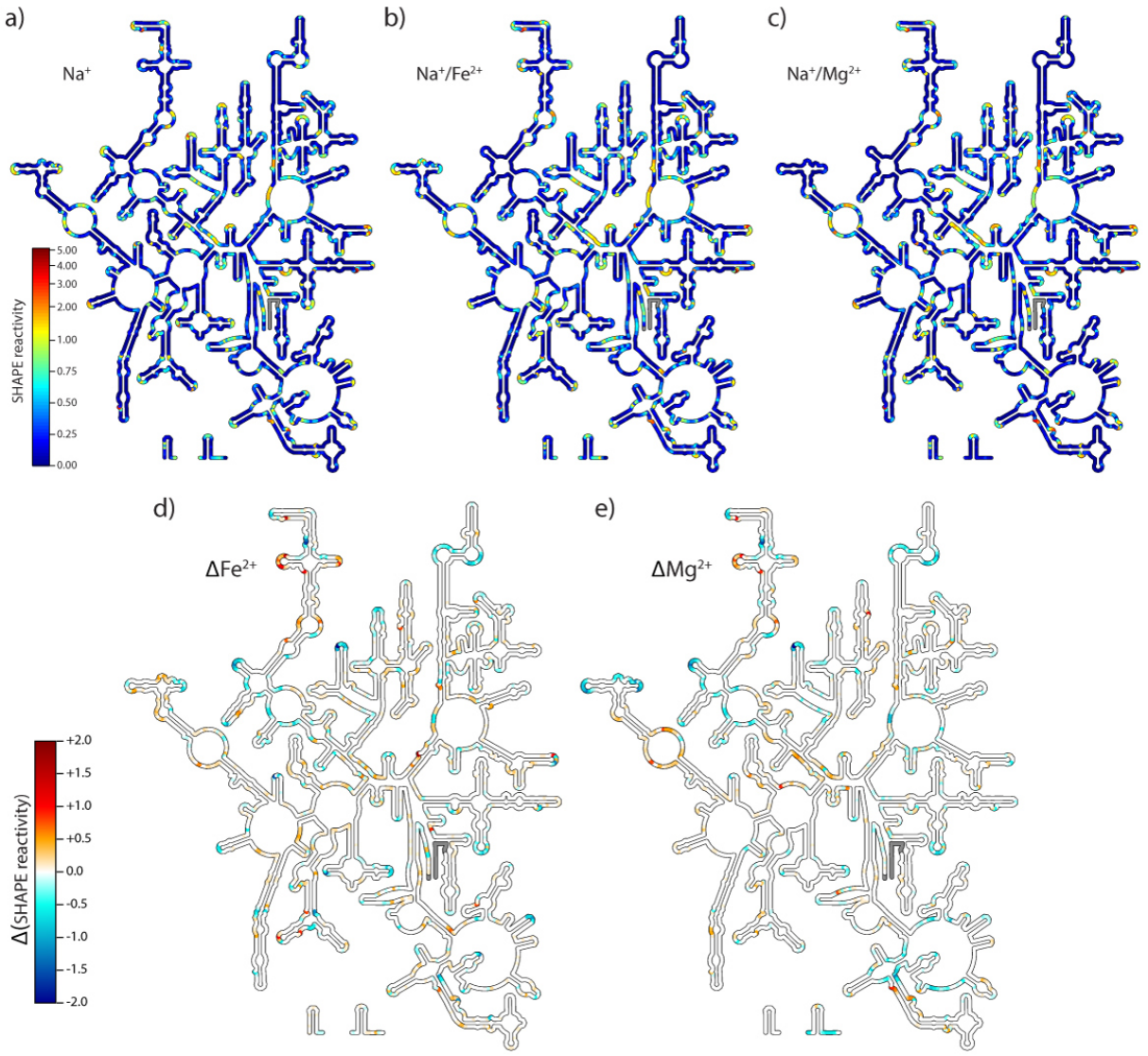
a)
Na+
b)
Na+/Fe2+
c)
Na+/Mg2+
SHAPE reactivity
5.00
4.00
3.00
2.00
1.00
0.75
0.50
0.25
0.00
d)
ΔFe2+
e)
ΔMg2+
Δ(SHAPE reactivity)
+2.0
+1.5
+1.0
+0.5
0.0
-0.5
-1.0
-1.5
-2.0

Figure 2

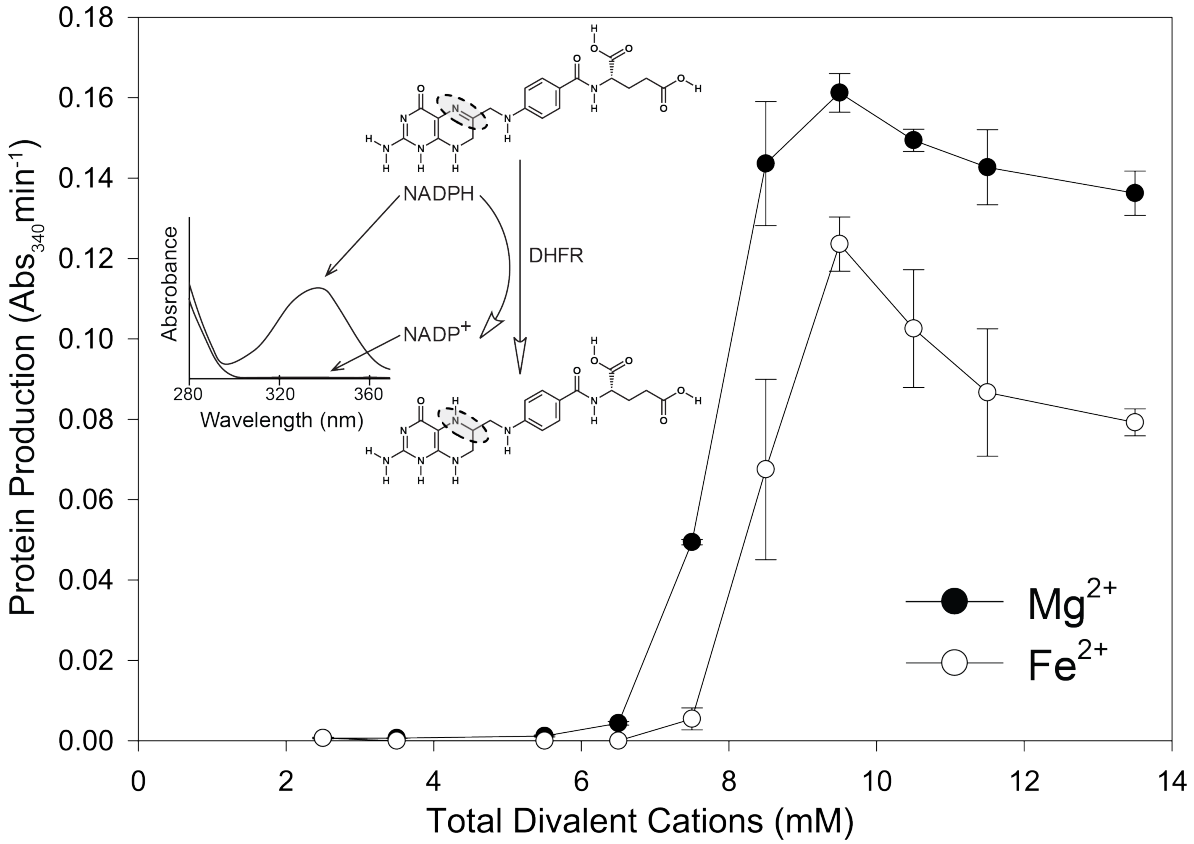

359 Figure 3
360

361

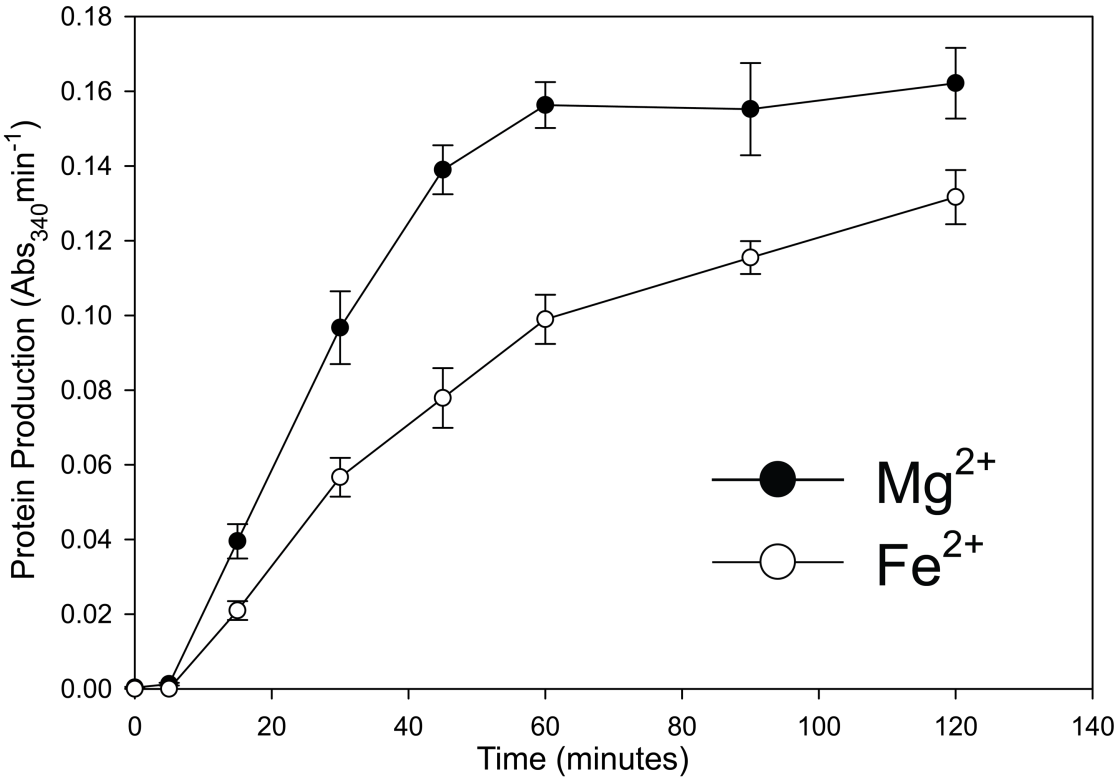

362
363 Figure 4
364

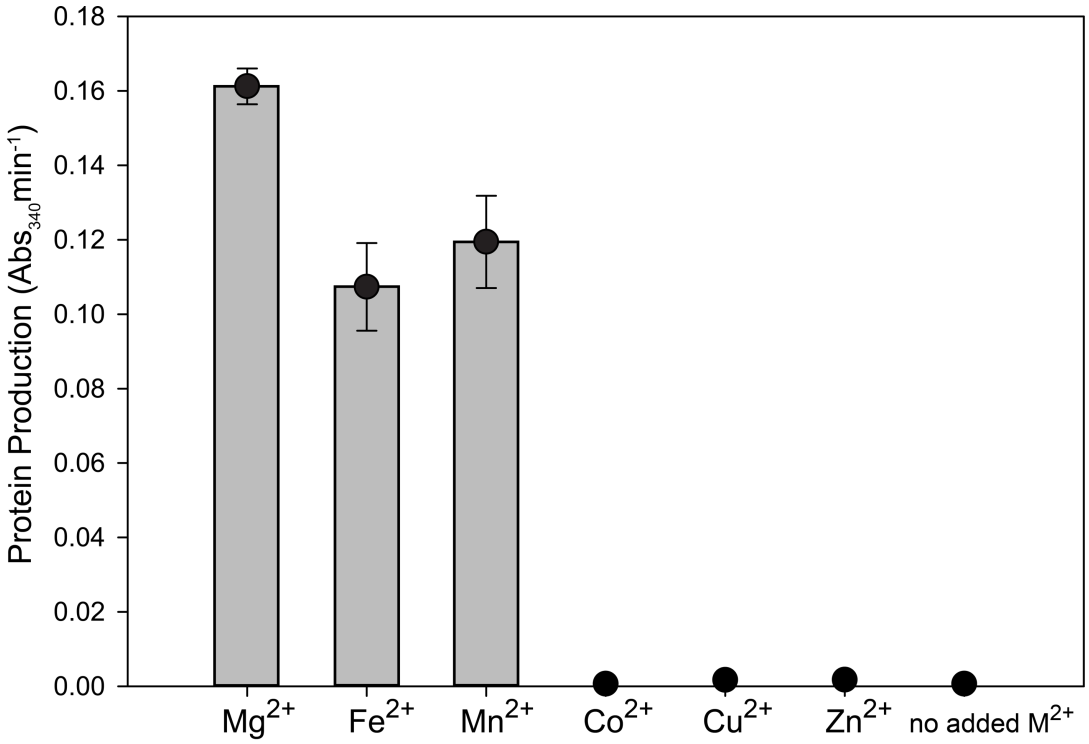

365
366
367 Figure 5